JOINT STATISTICS OF SOOT VOLUME FRACTION, PRIMARY PARTICLE DIAMETER AND TEMPERATURE IN FLAMES. PART I: EXPERIMENTAL SETUP

Zhiwei Sun[1,2,*], **Zeyad Alwahabi**[1,3], **Bassam Dally**[1,2], **Graham Nathan**[1,2]
*email: zhiwei.sun@adelaide.edu.au
[1]Centre for Energy Technology (CET), [2]School of Mechanical Engineering, and [3]School of Chemical Engineering, The University of Adelaide, SA 5005, Australia

Abstract

Simultaneous and planar measurements of flame temperature (T), soot volume fraction (f_v) and primary particle diameter (d_p) in forcing and turbulent sooting flames have been reported by our group. This paper particularly presents the core details of the experimental setup that combines non-linear two-line atomic fluorescence (nTLAF) and time-resolved laser-induced incandescence (TiRe-LII). The measurement accuracies and precisions are assessed. [1]

1. Introduction

There is an ongoing need for new techniques to achieve the simultaneous measurement of multiple critically important parameters in multiple dimensions in turbulent sooting flames, because of the non-linear and coupled interdependence between turbulence and chemistry. These parameters include flame temperature (T), soot volume fraction (f_v), mixture fraction and soot dimensions (primary particle diameter d_p, and aggregate size, R_{gm1}). Laser-based optical techniques are recognized as powerful tools, e.g. [1, 2, 3, 4, 5], although their application to turbulent sooting flames remains very challenging [6]. Indeed, even the measurement of f_v, using the relatively mature laser-induced incandescence (LII), requires substantial further development [7]. In addition, all of these parameters are coupled together in flames, with soot formation being a temperature dependent process and flame temperature being dependent on soot thermal radiation, which is a function of both f_v and d_p. Furthermore, in a turbulent flame, both the turbulence and chemistry are non-linear and also span some 10 orders of magnitude in length scale. Therefore, simultaneous measurement of all of the above parameters in multiple dimensions is desirable. Of these, the measurement of f_v, T and d_p in sooting flames are most advanced. However, their simultaneous, planar measurement with high spatial and temporal resolution had not been reported untill our recent two works [8, 9].

Compared with T and f_v, single-shot planar techniques to measure d_p are particularly under-developed. The so-called *RAYLIX* method, despite its attractiveness as a relatively simple technique, is of questionable accuracy because that the scattering behavior of soot aggregates is neglected [10, 11]. The method of combining LII and elastic light scattering (ELS) for simultaneous measurement of d_p, f_v and R_{gm1} is presently limited to point-wise detection [3, 12]. Time-resolved LII (TiRe-LII) has been widely used to measure d_p in flames, however, most previous TiRe-LII measurements are limited to pointwise detection or in steady flames without temporal resolution, e.g. [13, 14, 15, 16, 17, 18, 19, 20, 21, 22], which is of limited value in turbulent flames. Recently, Sun et al. demonstrated the single-shot imaging of d_p, simultaneously with f_v, in unsteady pre-mixed flames measured with planar TiRe-LII using four successive LII images, together with a model of the TiRe-LII process [23]. This work showed that d_p is very sensitive to local flame conditions. Cenker et al. performed

[1] A **Part II** is also presented in this conference, highlighting the significant values from the simultaneous, planar and quantitative measurements using this setup

two-time-step LII to image d_p in a high-pressure diesel combustion vessel, also together with a model, and compared the results with those obtained from thermophoretic sampling [24]. Their accompanying sensitivity analysis suggests that the accurate calculation of d_p from these parameters should employ a local and simultaneous measurement of flame temperature as an input to the model [25]. This is a point also discussed and identified elsewhere [13, 26]. For example, Hadef et al. incorporated flame temperature information, obtained from non-simultaneous coherent anti-Stokes Raman spectroscopy (CARS) measurements, in a gated TiRe-LII measurement [13]. However, no quantitative assessment of this correction is available in turbulent flames, even for point-wise TiRe-LII since this requires simultaneous measurement of flame temperature. This also motivated us to develop a nTLAF+TiRe-LII combined setup.

Several laser techniques have been explored for instantaneous measurement of T in sooting flames, such as filtered Rayleigh scattering (FRS) [27, 28], the widely used pointwise CARS [4, 13, 29, 30] and the novel planar CARS [31, 32], as well as two and two-line atomic fluorescence (TLAF) using atomic indium [33, 34]. Each of these methods are evolving rapidly with complementary strengths and limitations, so that each is likely to play important roles in advancing understanding of turbulent sooting flames. We have chosen TLAF working in non-linear saturation regime, i.e. nTLAF, for the present investigation because of its strong signal-to-noise ratio on the rich side of the reaction zone, where soot is present. Simultaneous imaging of T and f_v using nTLAF+LII has been demonstrated in both the unsteady laminar [35, 9] and highly turbulent soot flames [36, 8] by our group. Particularly in our recent works [8, 9] a new nTLAF setup, combined with TiRe-LII [23], was applied. The improvements in the new setup made the measurement of f_v in turbulent sooting flames with fuels of interest for research, such as ethylene, to be possible, where the peak value of f_v can reach up to 5 ppm [4, 5, 37]. However, core details of this nTLAF+TiRe-LII arrangement, details of data processing and the accuracy and precision of the method remain to be reported.

In light of the above background, the specific aims of the present investigation are (1) to present core details of the optical arrangement of the setup for single-shot, simultaneous measurement of f_v+T+d_p in two dimensions, (2) to present details of data processing and (3) to assess the precision and accuracy of the measurements.

2. Experimental and data processing

2.1 Burner and flames

An ethylene/air diffusion sooting flame was stabilized on a Santoro-type burner at atmospheric pressure. The burner consists of a 10.5 mm inner-diameter (ID) fuel pipe centered in an outer tube (ID = 97.7 mm). The central fuel tube extends 4 mm above the tip of the co-flow tube that houses stainless steel honeycombs (ID = 1 mm) for flow straightening. A steady, laminar and axis-symmetric sooting flame was generated. The fuel flow-rate was 0.183 ($\pm$0.003) standard liters per minutes (SLM) at 20 ^{o}C, while that for the outer air is 284 SLM, resulting in a flame of $\sim$64 mm in height. This flame is consistent with a flame reported previously [13], enabling the comparison of experimental data.

2.2 Optical setup

Figure 1 presents a schematic diagram of the optical setup, which is a combination of nTLAF and TiRe-LII. Two Nd:YAG pumped dye lasers were used to provide the excitation beams for nTLAF measurements, while signals were collected using two intensified CCD (ICCD) cameras. The fundamental output of a Nd:YAG laser (Brilliant B) was used in TiRe-LII measurements and four successive images were collected using an HSFC camera bundle.

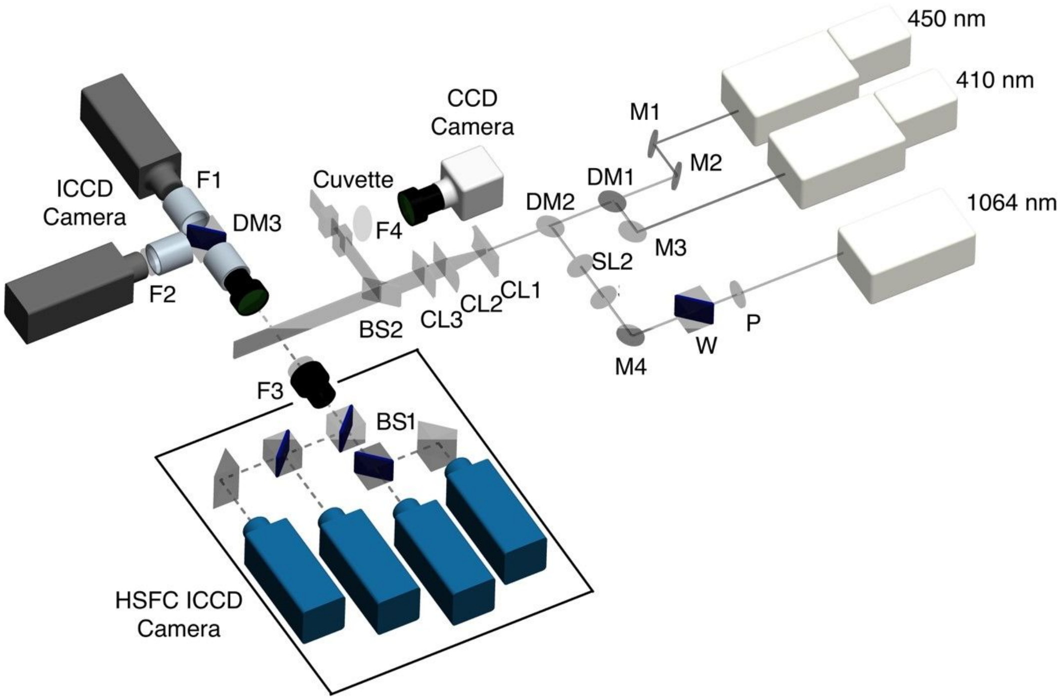

Figure 1: Schematic diagram of the experimental setup for the combined nTLAF and TiRe-LII measurements. **M**, mirror; **DM**, dichroic beam-splitter; **W**, half-wave plate; **P**, Glan-laser polarizer; **CL**, cylindrical lens; **SL**, spherical lens; **F**, band-pass filter; **BS**, prism beam splitter.

.

All lasers and cameras were externally trigged with an in-house timing system, and a timing feedback loop was used to synchronize all cameras. The lasers were fired at 10 Hz sequentially as $t_{laser@450nm} = 0$ ns, $t_{laser@410nm} = 120$ ns and $t_{laser@1064nm} = 1000$ ns. Indium particles were generated using a optical seeding system, not shown in Fig. 1, and transported to the flames following the fuel gas.

2.2.1 nTLAF

With nTLAF, the flame gas-phase temperature, T, is derived from the intensity ratio of two fluorescences from a tracer species (here atomic indium) sharing a common upper state, namely the Stokes and the anti-Stokes processes. This can be expressed as Eq. (1)

$$T = \frac{\frac{\Delta E}{k}}{ln\frac{G^{as}(I_{as})}{G^{s}(I_{s})} - ln\frac{F_{as}}{F_{s}} + C_T} \tag{1}$$

where the *sub-* and *super-*scripts s and as denote the Stokes and anti-Stokes processes, respectively. Here also, ΔE is the energy difference between the two lower states, k is Boltzmann's constant, F is the fluorescence intensity, I is the excitation laser fluence and the parameter C_T is a system-dependent calibration facto determind experimentally. Up to the regime of laser fluence, TLAF is grouped as linear TLAF [33], nTLAF [34] and saturated TLAF [38], for which the LIF signals as a function of laser flunece can be generally expressed as $F{=}a{\times}I/(1{+}b{\times}I)$. Considering the challenge in achieving homogeneous laser fluence on the cross section of a laser sheet, a general function of $F{=}G(I)$ may be more suitable applied in Eq. (1). The functions of G_a and G_{as} may not exactly follow the equation $F=a\times I/(1+b\times I)$, therefore, they were experimentally determined through a fitting process.

The present nTLAF arrangement generally follows the one described previously [34], but incorporates significant new features. The two excitation beams at 410.18 nm (Stokes) and 451.13 nm (anti-Stokes) had a temporal separation of ∼120 ns. They were combined with a dichroic mirror (DMLP425, Thorlabs) and reformed into a laser sheet of ∼350 μm thickness. The averaged laser fluence was kept at ∼0.03 J/cm^2 for both transitions, which is in the non-linear excitation regime. A higher laser fluence can potentially influence the subsequent TiRe-LII measurements at ∼1 μs later. The prism-based beam expanders in the dye laser oscillation cavities were removed to broaden the laser line width to increase the spectral overlap coefficients between the lasers and indium absorption. Up-beam from the flames, a small portion (∼10%) of the laser sheets was reflected into two cuvettes filled with distilled water and 300 nm (diameter) TiO_2 particles. Laser scattering was recorded with a CCD camera (MegaPlus, ES4020) to provide shot-to-shot corrections for variations in beam profiles.

Laser-induced fluorescence (LIF) of atomic indium was recorded using a new detection setup that comprises an image-splitter (TwinCam, Cairn) and two intensified CCD cameras (ICCD) through a 50 mm, f/1.2 lens. A long-pass dichroic beam-splitter (DMLP425, Thorlabs) was installed within the TwinCam image-splitter to separate the two LIF signals at 451.13 nm (Stokes) and 410.18 nm (ansti-Stokes). Two customize narrow-band pass filters (Alluxa) were employed to suppress laser-induced broadband interferences and laser scattering from soot [39], centered at 410.4 and 451.4 nm with a full-width at half maximum (FWHM) of 1.08 and 1.32 nm, respectively. These filters have a high optical density (OD>6.0) and >90% transmission. The system OD is estimated to be >8.0 at the laser wavelengths, taking into account the blocking function of the dichroic beam-splitter (DM3). The ICCD cameras (PI-MAX4, 1024f with GenIII *HBf* intensifiers) have quantum efficiency (QE) of 39% at 410 nm and of 50% at 451 nm. The in-plane spatial resolution of each camera images was 66×66 μm^2 and an integration time of 30 ns was chosen for both.

Micron- and nano-sized indium particles were seeded into the flames via a laser ablation setup [40, 41]. The power of the ablation laser (532 nm in wavelength and ∼6 ns in duration) was kept at 6 mJ/pulse at 10 Hz. No influence of either the ablation shocks or the indium seeding was detectable on either the flame shape or the LII images.

Calibrations for G_s, G_{as} functions and C_T factors in Eq. (1) were performed within the product zones of two non-sooting Bunsen-type ethylene/air flames burning 0.56 and 0.60 SLM ethylene premixed with 5.0 SLM air, respectively, stabilized on the same burner. In the calibration process of G_s, the fluence of the Stokes beam was varied using natural density filters, while that of the anti-Stokes beam was kept as constant. The intensities of Stokes fluorescence were firstly divided by the corresponding anti-Stokes signals to correct the variation of atomic indium concentration during data collection. The relationship between the corrected Stokes signals, i.e. the values of F_s/F_{as}, and the laser scattering intensity was fitted to get G_s in Eq. (1). The same process was also performed for the anti-Stokes process to get the G_{as} function. To calibrate the system factor C_T, the temperature of the two calibration flames needs to be assessed using alternative methods. In the present work, two methods were used. One was thermocouple measurement, in which a 75 μm *R*-type thermocouple (*R13R-003*, Omega) with a +61 K radiation correction was used. The other was the adiabatic flame temperatures calculated using the ChemKin software. It was found that adopting the first reference temperature (thermocouple results, ∼1900 K) in C_T calibration, nTLAF results in sooting flames were lower than previous results from CARS measurements, while those calibrated by the adiabatic temperatures (2202 and 2267 K) agreed well (as is shown in Section 3.1). This may be because the thermocouple is not suitable for measuring such high temperatures that are ∼2200 K. Therefore, all the data reported here was calibrated against the flame adiabatic temperatures.

Both the processes of calibration and temperature measurements have been performed *line-wise* across the laser sheets, i.e. row-by-row across all images. This can be understood as multiple line-wise nTLAF were performed simultaneously, and in each line-wise nTLAF the laser beam is approximately homogeneous spatially.

2.2.2 TiRe-LII

The TiRe-LII arrangement follows that described previously [23]. The four cameras were delayed at 0, 80, 160 and 240 ns relative to the laser with a same integration time of 30 ns. Prompt LII images were calibrated to deduce f_v, while images of d_p were evaluated from the delayed LII images by comparing with theoretical values calculated with a LII model [23, 42]. A filter transmitting 408-460 nm light (Brightline FF02-435/40, Semrock) was used to collect LII signals. The in-plane spatial resolution of each camera images was 85×85 μm^2.

The laser fluence was set to 0.30 J/cm^2 for all LII measurements. This value was chosen through the measurement of prompt LII intensity and soot temperature as a function of laser fluence. This laser fluence is sufficient to saturate soot particles of different size, but does not generate significant soot sublimation. Figure 2 presents the prompt LII signals in the steady sooting flame recorded simultaneously via two bandpass filters centered at 450 nm (FWHM: ±5 nm) and 700 nm (FWHM: ±20 nm). These were averaged over an area of 0.5×0.5 mm^2 both at the centerline (denoted *center*) and at the region with the maximum soot volume fraction in the wings (denoted *edge*) at height above the burner (HAB) of 25 mm, aiming to assess the influence of d_p on selection of LII laser fluence. Soot temperature was calculated from the two-color prompt LII signals. Figure 2 reveals that the saturation laser fluence is approximately the same in the two flame regions, though it is a little higher for small soot particles on the flame axis. At laser fluence ≥0.25 J/cm^2, although the maximum temperature of the large soot particles is higher than that of the small particles, the difference is within 200 K. In the fluence regime of greater than 0.25 J/cm^2), the maximum temperature of the heated particles is much less sensitive to the laser fluence than in the low fluence regime. It is noted that the relative spectral response of the two cameras was calibrated from the Abel-transformed flame luminosity with assuming an unexcited soot temperature of 1700 K. These may cause a small error in the soot temperatures reported in Fig. 2.

A beam (CW@1064 nm) extinction measurement was performed in the steady sooting flame to calibrate the LII images for f_v. A value of $K_e = 5.66$ was chosen for the dimensionless extinction coefficient. This value corresponds to $E(m) = 0.3$, where $E(m)$ is the soot refractive index. A look-up table of theoretical LII intensity ratios was generated as a function of both flame temperature T over $1200 \leqslant T_{flame} \leqslant 2400$ K in a step of 50 K and particle diameter d_p over the range of $5 \leqslant d_p \leqslant 100$ nm in a 5 nm step. This was generated for each image pair of S_2/S_1, S_3/S_1, S_4/S_1, S_3/S_2, S_4/S_2 and S_4/S_3, where S_i denotes the signal from the ith camera. The values of d_p were then calculated shot-by-shot from the LII ratios at the values closest the local flame temperature, also assuming non-aggregated soot particles and mono-disperse distribution of d_p, i.e. $\sigma_g = 0$. It was demonstrated to be possible to deduce both d_p and σ_g simultaneously from TiRe-LII signals [13], however, this is currently very challenging for instantaneous planar TiRe-LII due to the limited LII images. The mean of these six independent measurements was chosen to be representative of the local value of d_p.

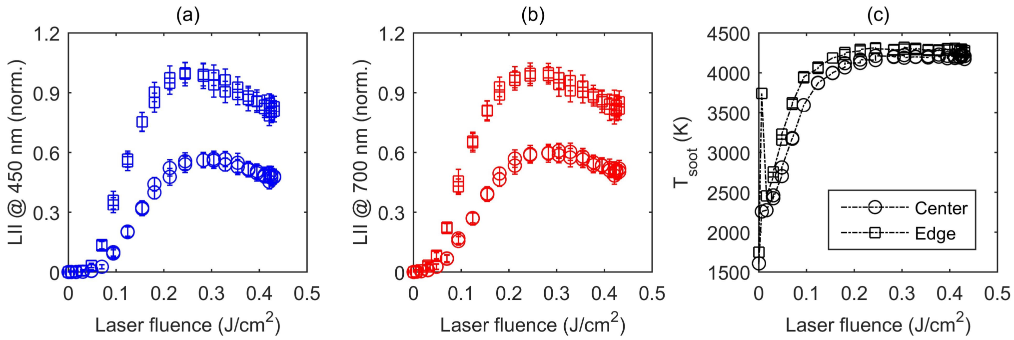

Figure 2: Normalized prompt LII signal intensities at (a) 450 nm and (b) 700 nm as a function of laser fluence, and (c) the corresponding soot initial temperature. LII signals were averaged over an area of 0.5×0.5 mm^2 on the centerline (denoted center) and at the region of maximum soot concentration in the wings (denoted *edge*) at a height of 25 mm in the steady flame. Signals were averaged from 100 simultaneous LII images.

3. Results and discussion

Figure 3 presents the images of T, f_v and d_p averaged over 100 single-shot measurements, together with the corresponding root-mean-squares (RMS). The averaged flame temperature was used in evaluating d_p. Temperature less than 1000 K could not be imaged due to the low LIF signals. Even in the region where f_v is approximately 5 ppm, laser-induced interferences were negligible. In Fig. 3, the distribution of T is much broader than that for f_v and d_p, to cover not only the sooting region but also substantial regions either side of it. This is a significant advantage of the nTLAF technique over soot or thin-filament pyrometry, e.g. [43]. Also, the width of the region of maximum measured d_p is significantly greater than that of the maximum f_v. This may be, in part, because the TiRe-LII technique is not sensitive in resolving large soot particles. The RMS of T is approximately 8% in the region with and upstream from sooting region, while it increases to ∼20% at the edge of the image with weak LIF signals there. The relatively large values of RMS for f_v and d_p in the downstream region is because of slight flame flicker. The typical RMS of the measured f_v is 8%, while that of d_p is 20%, which depends strongly on the magnitude of the LII signals (or f_v). The minimum RMS of d_p occurs in the wings where f_v is a maximum.

Figure 4 presents the radial profiles of the mean values measured at HAB = 30 mm. The curves clearly show the different locations where the three parameters peak. While it is expected that the peak value of T appears in the non-sooting region at $r = 4.4$ mm, the peak location of f_v appears at $r = 2.1$ mm. Interestingly, the profile of d_p is somewhat different from that of f_v. In the radial direction, d_p increases consistently with f_v before they simultaneously reach their peak values at $r = 2.1$ mm. After this location f_v decrease sharply because of the oxidation effect, while the decrease of d_p has a significant shift (∼1 mm), as shown in Fig. 4. The region of 2 mm$< r <$2.8 mm, where d_p is constant at its maximum value, is corresponding to the high gradient region of f_v. The flat-top region of d_p may be because the TiRe-LII is insensitive to large particles. Nevertheless, Fig. 4 clearly shows that approaching the oxidation region the decrease of d_p is delayed compared with that of f_v. This phenomenon was also found in our previous works [44, 23].

Figure 5 presents the probability distributions of T and d_p measured at $r = 0$ mm and 2.1 mm (where f_v peaks), respectively, both at HAB = 30 mm. The standard deviation (1σ) of T is ∼120 K. This variation is attributed to both the noise in the LIF images and the variation of laser modes. The precision of the d_p measurement is ∼11 nm (1σ) at $r = 0$ mm,

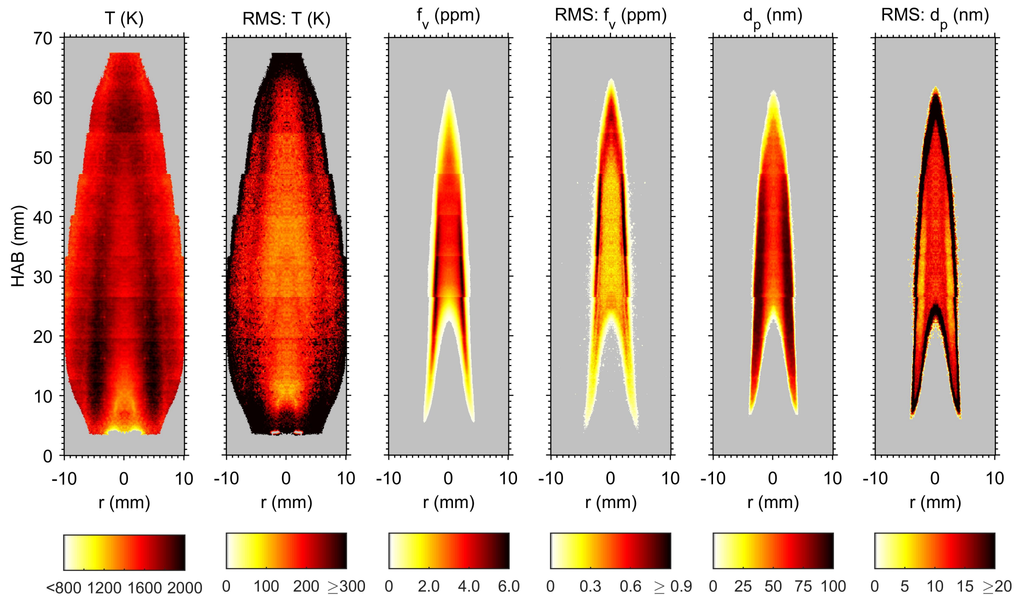

Figure 3: Images of the averaged T, f_v, and d_p, together with the corresponding RMS.

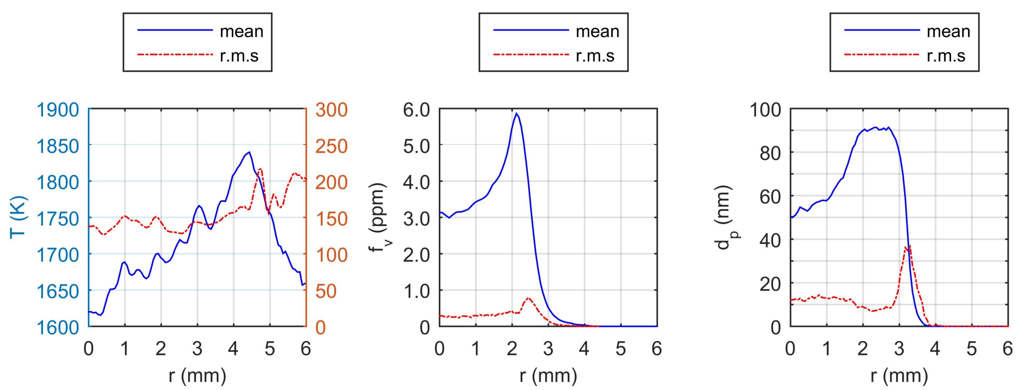

Figure 4: Radial profiles of the averaged T, f_v, and d_p, together with the corresponding RMS at height of 30 mm. The images are shown in Fig.3.

which is consistent with previous measurement ($\sigma = 9$ nm) in a premixed ethylene/air flame [23]. The precision at $r = 2.1$ mm with large d_p is similar (see Fig. 5d) and be noted that particles >100 nm are difficult to resolve using TiRe-LII. The significant difference between the mean value of d_p in Figs. 5c and 5d highlights the significant change of d_p in the flame.

Accuracies of T and d_p were assessed by comparison with previous results obtained in a very similar flame [13], where T was measured using CARS and d_p was measured using similar TiRe-LII by delaying the gate of a single ICCD camera, namely gated TiRe-LII. Figure 6 presents the results of T and d_p at three heights from two measurements, together with the present f_v results to indicate the sooting region. Qualitatively, the results of T are consistent. At $r = 0$ mm, temperature is lowest and increases with r, then peaks in the non-sooting oxidizing region. At HAB = 10 mm, T increases significantly in the radial direction, while at HAB = 50 mm the radial profile becomes much flatter. As shown in Fig. 6, the temperature results which were calibrated with the flame adiabatic temperatures (2261 and 2202 K) agree well with CARS measurements in sooting regions, but still with a maximum

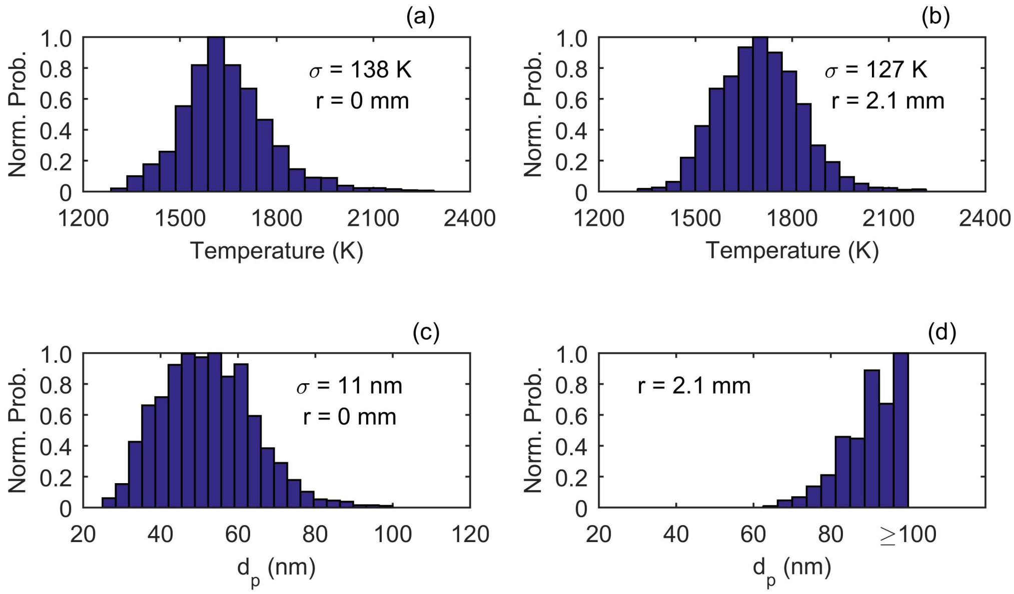

Figure 5: Normalized probability of T and d_p measured in the steady flame at HAB = 30 mm. The results are calculated from 100 single-shot measurements and over an area of $330 \times 330\ \mu m^2$ (55 pixels).

difference of 200 K in the oxidizing (non-sooting) region. The reason for this temperature difference in non-sooting regions needs to be assessed, nevertheless, it does not influence the relationships between soot and flame temperature derived from single-shot measurements. The measured temperatures calibrated with the thermocouple (not shown here) is always lower than that from the CARS measurement. This may be due to the temperatures (∼1940 and 1900 K) measured with the thermocouple are too low to be applicable. The accuracy of the nTLAF method is directly dependent on calibration, which further highlights the obvious need for an accurate calibration process, and a lower temperature flame may be more suitable for nTLAF calibration.

Figure 6 shows that the typical values of the measured d_p are greater, by approximately 2 times, than that reported previously [13] where the distribution of particle sizes (σ_g) were fitted simultaneously with d_p, and also greater than other previous measurements [45, 46]. This is partly attributed to the assumptions of a mono-disperse distribution of d_p and of non-aggregated soot particles, especially the latter assumption which can result in significant overestimation of d_p [23, 42] because soot particles are highly aggregated in this flame [45]. Qualitatively, the distributions of d_p are in good agreement, except that the previous measurements did not resolve well the gradients near to the edge of soot region. The present distributions of d_p are in good agreement with those measured in a longer but comparable ethylene/air diffusion flame [46]. Importantly, the present planar measurements reveal that the radial distribution of d_p is correlated with f_v at HAB = 10 mm. At HAB = 30 nm, d_p and f_v evolve consistently to their maximum values from $r = 0$ to 2 mm, but the rate of reduction in d_p is much lower than that of f_v beyond $r = 2$ mm, which is more clearly shown at HAB = 50 mm.

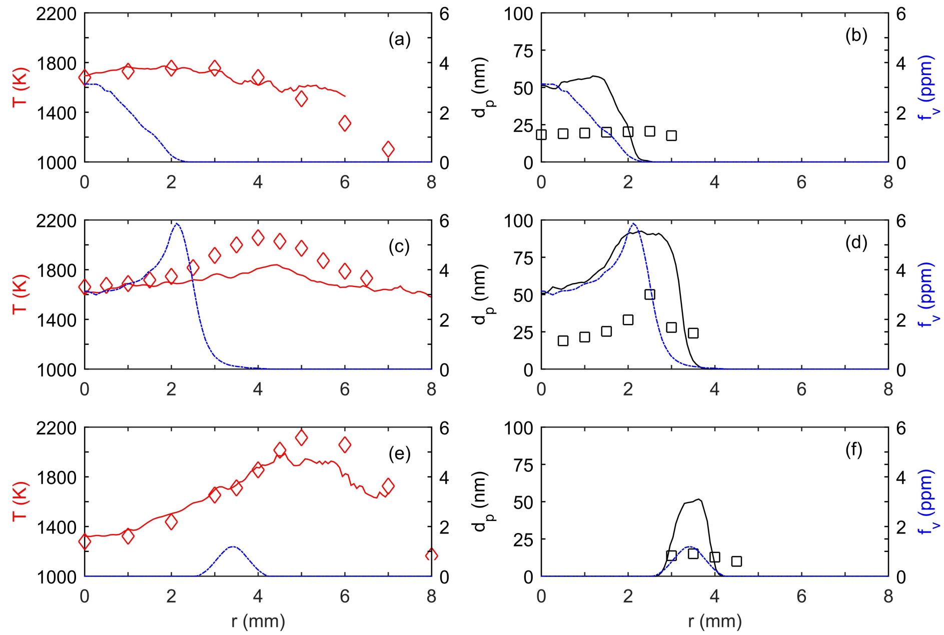

Figure 6: Radial profiles of the measured T, f_v and d_p at HAB=50 mm (**a** and **b**), 30 mm (**c** and **d**) and 10 mm (**e** and **f**). *Blue dash-dot* lines: the present measurements of f_v. *Res solid* lines: T and *Black solid* lines: d_p measured in this work. *Diamond*: T and *Square*: d_p, both from [13].

4. Conclusions

Single-shot, simultaneous imaging of T, f_v and d_p has been achieved in flames with peak f_v∼5 ppm, via an upgraded nTLAF+TiRe-LII setup. In single-shot measurements within a spatial resolution of 330×330 μm^2, it is found that: (1) the temperature results have a precision of ∼120 K and agree well with CARS measurements in the sooting region when nTLAF was calibrated against adiabatic flame temperatures, but are lower by ∼250 K in the non-sooting oxidizing region; (2) the measurement of f_v has a precision of 8%, while that for d_p is ∼20%, for a typical value of 11 nm. The d_p results are larger than those reported previously, by a factor of ∼2, partly because particle aggregation has not been taken into account; and (3) significant spatial profiles of T, f_v and d_p can be derived from single shot images with this system, which was not possible from previous arrangements.

Acknowledgments

The Australia Research Council is gratefully acknowledged for financial support (DP130100198). The authors thank Dr. Dahe Gu and Mr. KaeKen Foo for their assistance in the experiment.

References

[1] Geigle, K., OLoughlin, W., Hadef, R., Meier, W., "Visualization of soot inception in turbulent pressurized flames by simultaneous measurement of laser-induced fluorescence of polycyclic aromatic hydrocarbons and laser-induced incandescence, and correlation to oh distributions", *Appl. Phys. B* 119:717–730 (2015).

[2] Franzelli, B., Scouflaire, P., Candel, S., "Time-resolved spatial patterns and interactions of soot, pah and oh in a turbulent diffusion flame", *Proc. Combust. Inst.* 35:1921–1929 (2015).

[3] Crosland, B.M., Thomson, K.A., Johnson, M.R., "Simultaneous instantaneous measurements of soot volume fraction, primary particle diameter, and aggregate size in turbulent buoyant diffusion flames", *Proc. Combust. Inst.* 35:1851–1859 (2015).

[4] Köhler, M., Geigle, K.P., Meier, W., Crosland, B.M., Thomson, K.A., Smallwood, G.J., "Sooting turbulent jet flame: characterization and quantitative soot measurements", *Appl. Phys. B* 104:409–425 (2011).

[5] Shaddix, C.R., Zhang, J., Schefer, R.W., Doom, J., Oefelein, J.C., Kook, S., Pickett, L.M., Wang, H., "Understanding and predicting soot generation in turbulent non-premixed jet flames", Report, Sandia National Laboratoies (2010).

[6] Nathan, G.J., Kalt, P.A.M., Alwahabi, Z.T., Dally, B.B., Medwell, P.R., Chan, Q.N., "Recent advances in the measurement of strongly radiating, turbulent reacting flows", *Prog. Energ. Combust* 38:41–61 (2012).

[7] Michelsen, H.A., Schulz, C., Smallwood, G.J., Will, S., "Lii: Particulate diagnostics for combustion, atmospheric, and industrial applications", *Prog. Energ. Combust.* 51:2–48 (2015).

[8] Gu, D., Sun, Z., Dally, B.B., Medwell, P.R., Alwahabi, Z.T., Nathan, G.J., "Simultaneous measurements of gas temperature, soot volume fraction and primary particle diameter in a sooting lifted turbulent ethylene/air non-premixed flame", *Combust. Flame* 179:33 – 50 (2017).

[9] Foo, K.K., Sun, Z., Medwell, P.R., Alwahabi, Z.T., Dally, B.B., Nathan, G.J., "Experimental investigation of acoustic forcing on temperature, soot volume fraction and primary particle diameter in non-premixed laminar flames", *Combust. Flame* 181:270 – 282 (2017).

[10] Bockhorn, H., Geitlinger, H., Jungfleisch, B., Lehre, T., Schon, A., Streibel, T., Suntz, R., "Progress in characterization of soot formation by optical methods", *Phys Chem Chem Phys* 4:3780–3793 (2002).

[11] Geitlinger, H., Streibel, T., Suntz, R., Bockhorn, H., "Two-dimensional imaging of soot volume fractions, particle number densities, and particle radii in laminar and turbulent diffusion flames", *Proc. Combust. Inst.* 27:1613–1621 (1998).

[12] Crosland, B.M., Thomson, K.A., Johnson, M.R., "Instantaneous in-flame measurement of soot volume fraction, primary particle diameter, and aggregate radius of gyration via auto-compensating lii and two-angle elastic light scattering", *Appl. Phys. B* 112:381–393 (2013).

[13] Hadef, R., Geigle, K., Zerbs, J., Sawchuk, R., Snelling, D., "The concept of 2d gated imaging for particle sizing in a laminar diffusion flame", *Appl. Phys. B* 112:395–408 (2013).

[14] Menkiel, B., Donkerbroek, A., Uitz, R., Cracknell, R., Ganippa, L., "Measurement of in-cylinder soot particles and their distribution in an optical hsdi diesel engine using tr-lii", *Combust. Flame* 159:2985–2998 (2012).

[15] Bladh, H., Johnsson, J., Olofsson, N.E., Bohlin, A., Bengtsson, P.E., "Optical soot characterization using 2c-lii in the soot growth region of a premixed flat flame", *Proc. Combust. Inst.* 33:641–648 (2011).

[16] Ryser, R., Gerber, T., Dreier, T., "Soot particle sizing during high-pressure diesel spray combustion via tire-lii", *Combust. Flame* 156:120–129 (2009).

[17] Banerjee, S., Menkiel, B., Ganippa, L.C., "Multi-lognormal soot particle size distribution for tire-lii in diesel engines", *Appl. Phys. B* 96:571–579 (2009).

[18] Hofmann, M., Kock, F., Dreier, T., Jander, H., Schulz, C., "Lii for soot-particle sizing at elevated pressure", *Appl. Phys. B* 90:629–639 (2008).

[19] Kock, B.F., Tribalet, B., Schulz, C., Roth, P., "2c tire-lii applied to soot particle sizing in the cylinder of a diesel engine", *Combust. Flame* 147:79–92 (2006).

[20] Lehre, T., Suntz, R., Bockhorn, H., "Time-resolved two-color lii: size distributions of nano-particles from gas-to-particle synthesis", *Proc. Combust. Inst.* 30:2585–2593 (2005).

[21] Schittkowski, T., Mewes, B., Bruggemann, D., "Lii and raman measurements in sooting methane and ethylene flames", *Phys Chem Chem Phys* 4:2063–2071 (2002).

[22] Will, S., Schraml, S., Leipertz, A., "Two-dimensional soot-particle sizing by tire-lii", *Opt. Lett.* 20:2342–2344 (1995).

[23] Sun, Z.W., Gu, D.H., Nathan, G.J., Alwahabi, Z.T., Dally, B.B., "Single-shot, time-resolved planar laser-induced incandescence (tire-lii) for soot primary particle sizing in flames", *Proc. Combust. Inst.* 35:3673–3680 (2015).

[24] Cenker, E., Kondo, K., Bruneaux, G., Dreier, T., Aizawa, T., Schulz, C., "Assessment of soot particle-size imaging with lii at diesel engine conditions", *Appl. Phys. B* 119:765–776 (2015).

[25] Cenker, E., Bruneaux, G., Dreier, T., Schulz, C., "Sensitivity analysis for soot particle size imaging with lii at high pressure", *Appl. Phys. B* pp. 1–19 (2015).

[26] Schraml, S., Dankers, S., Bader, K., Will, S., Leipertz, A., "Soot temperature measurements and implications for tire-lii", *Combust. Flame* 120:439–450 (2000).

[27] Hofmann, D., Leipert, A., "Temperature field measurements in a sooting flame by filtered rayleigh scattering (frs)", *Proc. Combust. Inst.* 26:945–950 (1996).

[28] Kearney, S.P., Schefer, R.W., Beresh, S.J., Grasser, T.W., "Temperature imaging in nonpremixed flames by joint filtered rayleigh and raman scattering", *Applied Optics* 44:1548–1558 (2005).

[29] Kliewer, C.J., Gao, Y., Seeger, T., Kiefer, J., Patterson, B.D., Settersten, T.B., "Picosecond time-resolved pure-rotational cars in sooting flames", *Proc. Combust. Inst.* 33:831–838 (2011).

[30] Glder, .L., Snelling, D.R., Sawchuk, R.A., "Influence of hydrogen addition to fuel on temperature field and soot formation in diffusion flames", *Proceedings of the Combustion Symposium* 26:2351–2358 (1996).

[31] Bohlin, A., Kliewer, C.J., "Communication: 2d-cars: Simultaneous planar imaging and multiplex spectroscopy in a single laser shot", *J Chem Phys* 138 (2013).

[32] Bohlin, A., Kliewer, C.J., "Direct coherent raman temperature imaging and wideband chemical detection in a hydrocarbon flat flame", *The Journal of Physical Chemistry Letters* 6:643–649 (2015).

[33] Engstrm, J., Nygren, J., Aldn, M., Kaminski, C.F., "Two-line atomic fluorescence as a temperature probe for highly sooting flames", *Opt Lett* 25:1469–1471 (2000).

[34] Medwell, P.R., Chan, Q.N., Kalt, P.A.M., Alwahabi, Z.T., Dally, B.B., Nathan, G.J., "Development of temperature imaging using tlaf", *Applied Optics* 48:1237–1248 (2009).

[35] Chan, Q.N., Medwell, P.R., Kalt, P.A.M., Alwahabi, Z.T., Dally, B.B., Nathan, G.J., "Simultaneous imaging of temperature and soot volume fraction", *Proc. Combust. Inst.* 33:791–798 (2011).

[36] Mahmoud, S.M., Nathan, G.J., Medwell, P.R., Dally, B.B., Alwahabi, Z.T., "Simultaneous planar measurements of temperature and soot volume fraction in a turbulent non-premixed jet flame", *Proc. Combust. Inst.* 35:1931–1938 (2015).

[37] Köhler, M., Geigle, K.P., Blacha, T., Gerlinger, P., Meier, W., "Experimental characterization and numerical simulation of a sooting lifted turbulent jet diffusion flame", *Combust. Flame* 159:2620–2635 (2012).

[38] Manteghi, A., Shoshin, Y., Dam, N.J., de Goey, L.P.H., "Two-line atomic fluorescence thermometry in the saturation regime", *Applied Physics B* 118:281–293 (2015).

[39] Gu, D., Sun, Z., Nathan, G.J., Medwell, P.R., Alwahabi, Z.T., Dally, B.B., "Improvement of precision and accuracy of temperature imaging in sooting flames using tlaf", *Combust. Flame* 167:481–493 (2016).

[40] Gu, D.H., Sun, Z.W., Medwell, P.R., Alwahabi, Z.T., Dally, B.B., Nathan, G.J., "Mechanism for lif signal generation in a nanoparticle-seeded flow for planar flame thermometry", *Appl. Phys. B* 118:209–218 (2015).

[41] Medwell, P.R., Chan, Q.N., Dally, B.B., Alwahabi, Z.T., Mahmoud, S., Metha, G.F., Nathan, G.J., "Flow seeding with elemental metal species via an optical method", *Appl. Phys. B* 107:665–668 (2012).

[42] Bladh, H., Johnsson, J., Bengtsson, P.E., "On the dependence of lii signal on soot volume fraction for variations in particle size", *Appl. Phys. B* 90:109–125 (2008).

[43] Kempema, N.J., Long, M.B., "Quantitative rayleigh thermometry for high background scattering applications with structured laser illumination planar imaging", *Applied Optics* 53:6688–6697 (2014).

[44] Sun, Z., Dally, B., Nathan, G., Alwahabi, Z., "Effects of hydrogen and nitrogen on soot volume fraction, primary particle diameter and temperature in laminar ethylene/air diffusion flames", *Combust. Flame* 175:270 – 282 (2017).

[45] Tian, K., Liu, F., Thomson, K.A., Snelling, D.R., Smallwood, G.J., Wang, D., "Distribution of the number of primary particles of soot aggregates in a nonpremixed laminar flame", *Combust. Flame* 138:195–198 (2004).

[46] D'Anna, A., Rolando, A., Allouis, C., Minutolo, P., DAlessio, A., "Nano-organic carbon and soot particle measurements in a laminar ethylene diffusion flame", *Proc. Combust. Inst.* 30:1449–1456 (2005).